Low-energy suspension structure of a magnetorheological fluid

Joanne H. E. Promislow [1] and Alice P. Gast [1,2]
[1] *Department of Chemistry, Stanford University, Stanford, California 94305*
[2] *Department of Chemical Engineering, Stanford University, Stanford, California 94305*
(Received 4 September 1996)

The application of a pulsed magnetic field to an emulsion of monodisperse, magnetizable oil droplets yields an energetically determined suspension structure. For droplets with a radius $r \geqslant 0.32$ μm and a magnetic susceptibility of $\chi = 2.2$, the low-energy suspension structure comprises ellipsoidal aggregates with conical spikes. The eccentricity of the ellipsoidal aggregates can be explained primarily by a competition between demagnetizing field and surface effects. Calculations of the equilibrium ellipsoid width-to-length ratio based on these two dipolar forces, as well as the relatively minor effects of interaggregate repulsion and gravity, provide good agreement with experimental observations of aggregate shape. The formation of conical spikes on the aggregate ends results from a surface energy anisotropy that forbids surfaces perpendicular to the field direction. A comparison of the narrow range of observed spike sizes with surface energy anisotropy calculations suggests that surfaces are stable only when the ratio of the surface energy to the dipolar energy driving chain formation exceeds a critical value. A slight dependence of the range of allowable spike sizes on pulse frequency is observed and could arise from a variation in the internal structure of the aggregates with pulse frequency. [S1063-651X(97)00207-9]

PACS number(s): 82.70.−y

I. INTRODUCTION

Magnetorheological (MR) fluids are suspensions of paramagnetic particles in a nonmagnetic fluid. When a magnetic field is applied to a MR fluid, the particles acquire a dipole moment aligned with the external field and aggregate tip to tip to form chains parallel to the applied field. At high particle volume fractions, these chains cross-link and the suspension effectively solidifies [1]. Due to this capability for a rapid rheological response, MR fluids have the potential to revolutionize electromechanical interfaces and are a subject of great interest. Current commercial MR fluid products include tunable dampers and brakes, while future applications in robotics, clutches, and a host of vibration-control systems are envisioned [2,3].

Most studies of MR fluids to date have focused on their response to a continuous (dc) field. When exposed to a strong, continuous magnetic field, concentrated MR fluids rapidly form a cross-linked network. This fibrous network is capable of supporting a stress and is the desired structure when increased resistance is needed; it is not, however, the lowest-energy suspension structure. The continuous-field structure is determined by the kinetics of aggregation and particles are prohibited from rearranging to minimize energy as long as the field persists. In contrast, we recently found that the application of a pulsed field (square wave alternating between field-on and field-off states) to a MR fluid does produce an energetically determined suspension structure [4]. By allowing particle diffusion during the field-off state, a pulsed field enables minimization of energy through structural rearrangements. In dramatic contrast to the cross-linked network that results from the application of a continuous field, we discovered that for particles with a magnetic susceptibility of $\chi = 2.2$ and radius $r \geqslant 0.32$ μm, the low-energy suspension structure produced by a pulsed magnetic field comprises ellipsoidal aggregates with spiked ends. Having access to this energetically relaxed state is extremely valuable for the information it gives about the structure-determining competition between the dipolar interactions in a MR fluid.

In this paper we present an analysis of the low-energy MR fluid suspension structure consisting of ellipsoidal aggregates with conical tips. We begin by reviewing the evolution of suspension structure in a MR fluid exposed to a pulsed magnetic field. We then calculate the equilibrium eccentricity of an ellipsoidal aggregate by incorporating the effects of the demagnetizing field, surface energy, interaggregate repulsion, and gravity and compare our results with experimental measurements. In Sec. III, we analyze the formation of the conical spikes by interpreting our experimental findings in the context of the surface energy anisotropy calculations performed by Lobkovsky and Halsey [5]. We also present information on the effects of pulse frequency on spike angle.

II. ELLIPSOID ECCENTRICITY

A. Experimental motivation

We studied an emulsion of ferrofluid-containing oil droplets dispersed in water and stabilized against irreversible aggregation by sodium dodecyl sulfate. The ferrofluid, a Rhône-Poulenc product provided by J. Bibette, is in the form of small grains of 100-Å single magnetic domains of the iron oxide Fe_2O_3 dispersed in octane at 19% by volume. The iron oxide domains are ferromagnetic, but since no long-range order exists between domains, the droplets are superparamagnetic; their magnetization is completely reversible and, at low field strengths, is proportional to the external field through χ the effective magnetic susceptibility. Using a fractionation procedure developed by Bibette [6], we synthesized and fractionated the emulsions into very monodisperse and stable fractions ranging in droplet size from a radius of 0.05 μm to 0.5 μm. For the experiments discussed in this paper

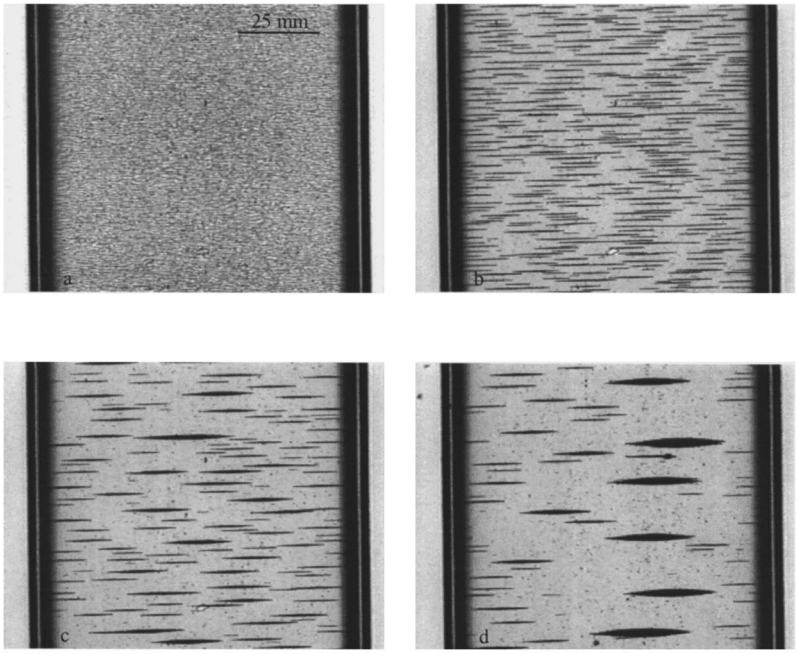

FIG. 1. Suspension structure of a MR fluid sample with a droplet volume fraction of $\phi = 0.005$ and particle radius of $r = 0.32$ μm (a) 1 s, (b) 3 min, (c) 15 min, and (d) 1 h after the application of a pulsed magnetic field of strength $H = 1480$ A/m ($\lambda = 37$) and pulse frequency $\nu = 2.0$ Hz. The field direction is parallel to the long axis of the aggregates.

we used samples with a droplet radius r of 0.32 μm and a droplet magnetic susceptibility χ of 2.2.

The suspensions are held on a microscope stand in sealed microrectangular tubes, 50 μm$\times$ 1 mm in cross section and 50 mm in length. A uniform magnetic field is generated in the sample by two coils of copper wire placed one on each side of the sample. After application of the magnetic field, the evolution of suspension structure is recorded with a charge coupled device video camera and digital images, consisting of 510×492 pixels with 256 gray levels, are obtained for analysis.

When the magnetic field is applied, the emulsion droplets acquire dipole moments $\mu = \frac{4}{3}\pi r^3 \mu_0 \chi H$, where r is the particle radius, μ_0 is the magnetic permeability of a vacuum, and H is the external field. The interaction energy $U(x,\theta)$ between two droplets with aligned, identical dipole moments is

$$U(r,\theta) = \frac{\mu^2}{4\pi\mu_0}\frac{1-3\cos^2\theta}{x^3}, \tag{1}$$

where x is the distance between sphere centers and θ is the angle between the applied field and the line joining the sphere centers. The dimensionless dipole strength λ provides a ratio of the maximum magnetic attraction between two droplets (i.e., droplets touching and aligned with the external field) to the thermal energy

$$\lambda = \frac{-U_{\max}}{kT} = \frac{\pi\mu_0 r^3 \chi^2 H^2}{9kT}. \tag{2}$$

The structural rearrangements that accompany the minimization of energy in a MR fluid sample are illustrated in Fig. 1, which shows the effects of a pulsed magnetic field of strength $H = 1480$ A/m, corresponding to $\lambda = 37$, and frequency $\nu = 2.0$ Hz on a sample with droplet volume fraction $\phi = 0.005$. Figure 1(a) is an image of the cross-linked network that forms in an immediate kinetically driven response to the applied field. This network quickly disintegrates in the pulsed field as the droplets are energetically driven into concentrated and depleted regions. The originally rather columnar aggregates then slowly rearrange into their final ellipsoidal shape [Fig. 1(d)]. Figure 2 shows a magnified view of the final shape of the energetically relaxed aggregates. Our goal in Sec. II B is to calculate the equilibrium aggregate shape based on what we believe are the most important structure-determining forces and compare the calculated low-energy shape with our experimental results to gauge how well we truly understand the interplay of forces in a MR fluid aggregate.

B. Calculations: Model

Various dipolar interactions compete to determine the most energetically favorable aggregate shape in a MR fluid. The three primary structure-determining interactions are the demagnetizing field, the surface energy, and the repulsive

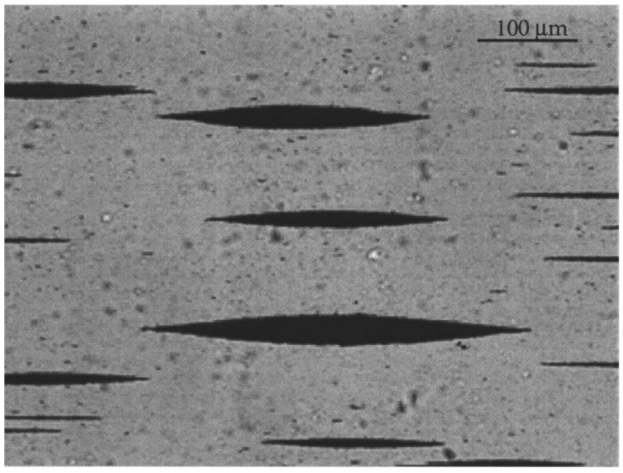

FIG. 2. Magnified view of aggregates formed under the same experimental conditions as in Fig. 1(d).

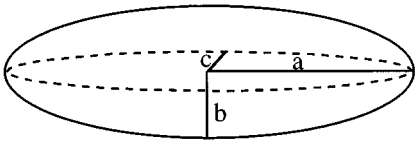

FIG. 3. Ellipsoid of semilength a, semiwidth b, and semithickness c with $a \geqslant b \geqslant c$. The external field is parallel to the a axis and gravity is parallel to the c axis.

interaction between aggregates [7,8]. The demagnetizing field forms inside a magnetizable ellipsoid exposed to an external magnetic field. Its direction always opposes that of the applied field; the demagnetizing field therefore weakens the total field inside the ellipsoid and consequently increases the aggregate energy. Minimizing the demagnetizing field favors the formation of long, thin aggregates. The surface energy arises from the fact that particles on the surface of the aggregate experience a weaker local field than particles in the bulk and consequently contribute less to the total aggregate dipole moment. Since a greater aggregate dipole moment corresponds to a lower aggregate energy, creating a surface costs energy and minimizing the surface energy thus favors decreasing the surface area by adopting a more spherical shape. The repulsive interaction between aggregates favors increasing the interaggregate separation distance by forming fewer, bigger aggregates rather than smaller, more closely spaced aggregates.

All theories that have been developed to calculate the lowest-energy structure of a system of interacting dipolar colloids have been based on all or some of these three dipolar interactions [7–10]. In all cases, the aggregate length was assumed to be invariant and equal to the cell length in the field direction. Only the dependence of aggregate width and interaggregate separation on aggregate length has been calculated. It is clear from our experiments, however, that the equilibrium aggregate length is not necessarily fixed by the cell dimensions. We decided therefore to perform calculations of the most energetically favorable aggregate eccentricity by incorporating the effects of the demagnetizing field, the surface energy, and the interaggregate repulsion. A comparison of the calculated results with our experimental measurements could then be used to test the validity of equilibrium properties determined by theories based primarily on these dipolar interactions.

We begin by reviewing the derivation of the equation for the total suspension energy. In order to render calculation of the demagnetizing field tractable, we model the aggregates as ellipsoids of semilength a, semiwidth b, and semithickness c with the axis a parallel to the external magnetic field, the axis c parallel to gravity, and the axis b perpendicular to both the field and gravity and $a \geqslant b \geqslant c$, as shown in Fig. 3. The total energy U_T for a suspension of ellipsoidal aggregates of magnetizable material in an external magnetic field $\mathbf{H}$ is given by [11]

$$U_T = -\frac{N\mathbf{m}_a \cdot \mathbf{H}}{2}, \tag{3}$$

where N is the number of aggregates and $\mathbf{m}_a$ is the magnetic moment of an aggregate. The demagnetizing field, the surface energy, and the interaggregate interaction all influence $\mathbf{m}_a$.

An isolated ellipsoid of a homogeneous magnetic medium has a magnetic moment $\mathbf{m}_h$ given by

$$\mathbf{m}_h = \mu_0 V_a \left[\frac{\chi_a \mathbf{H}}{1 + (4\pi\chi_a) n_z} \right], \tag{4}$$

with V_a the aggregate volume, χ_a the average magnetic susceptibility of the aggregate, and n_z the demagnetizing factor that accounts for the strength of the internal demagnetizing field. We determine χ_a from the magnetic susceptibility of the droplets χ_d, the magnetic susceptibility of the medium χ_m, in this case water, and the volume fraction of droplets in an aggregate ϕ_a using Bruggeman's model for spherical inclusions [12]:

$$\left(\frac{\chi_a - \chi_d}{\chi_m - \chi_d} \right) \left(\frac{1 + 4\pi\chi_m}{1 + 4\pi\chi_a} \right)^{1/3} = 1 - \phi_a . \tag{5}$$

Assuming random close packing ($\phi_a = 0.64$), with $\chi_d = 2.2$ and $\chi_m = 0$, we thus obtain $\chi_a = 0.58$.

The demagnetizing factor n_z is determined solely by the shape of the ellipsoidal aggregate, decreasing as the ellipsoid elongates. For an ellipsoid of revolution ($b = c$ in Fig. 3), the demagnetizing factor is given simply by [11]

$$n_z = \left[\frac{1 - e^2}{2e^3} \right] \left[\ln\left(\frac{1+e}{1-e} \right) - 2e \right], \tag{6}$$

with $e = (1 - b^2/a^2)^{1/2}$ the ellipsoid eccentricity. Since we cannot assume that an ellipsoid of revolution is the most favorable aggregate shape and we are unable to experimentally determine the thickness of our aggregates, we use the full form of the equation for the demagnetizing factor to allow calculation of the aggregate energy for all possible ellipsoidal shapes. Setting $\beta = b/a$ and $\gamma = c/a$ (thus $1 \geqslant \beta \geqslant \gamma$), the demagnetizing factor can be expressed as [13]

$$n_z = \frac{\beta\gamma}{(1-\gamma^2)^{1/2}(1-\beta^2)} \{ F(k,\varphi) - E(k,\varphi) \}, \tag{7}$$

where $F(k,\varphi)$ and $E(k,\varphi)$ are incomplete elliptic integrals of the first and second kind, respectively, $k^2 = (1-\beta^2)/(1-\gamma^2)$ and $\sin^2\varphi = 1 - \gamma^2$. We numerically evaluate the elliptic integrals using the arithmetic-geometric mean method [14]. The demagnetizing factor is plotted as a function of β and γ in Fig. 4. Notice that the demagnetizing factor depends on the relative rather than the absolute lengths of the semiaxes and increases with both increasing β and γ.

Following Grasselli *et al.* [8], we next incorporate the effects of the surface energy and the repulsive interaction between aggregates into the total-energy calculation. As mentioned previously, the surface energy derives from the droplets on the surface of the aggregate experiencing a weaker local field than droplets in the bulk due to the absence of magnetization from surrounding droplets on half of the spherical surface of a droplet on the aggregate surface. The dipole moment of a droplet on the surface is thus weaker than the dipole moment of a bulk droplet by an amount $\delta\mathbf{m}$ and the actual aggregate dipole moment $\mathbf{m}_a$ is reduced

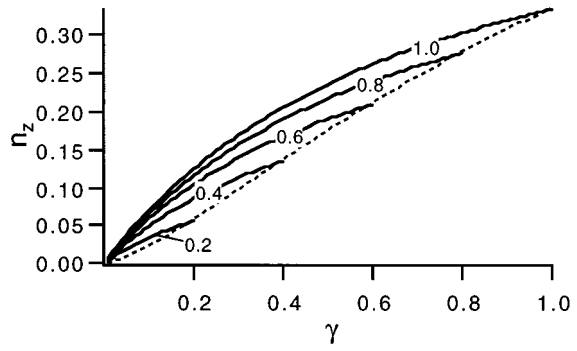

FIG. 4. Demagnetizing factor as a function of γ for β values of 0.2, 0.4, 0.6, 0.8, and 1.0 indicated on the curves. The dashed line is the curve for $\beta=\gamma$.

from the homogeneous value $\mathbf{m}_h$ by an amount $\mathbf{m}_s=N_s\delta\mathbf{m}$, where N_s is the number of droplets on the surface. Although the surface energy is dependent on the configuration of the first two or three particle layers below the surface, we consider only the first layer since lattice model calculations have shown the contribution from this surface layer to be far greater than all others [15].

Although the value of $\delta\mathbf{m}$ is sensitive to the precise structure of the surface and is generally anisotropic as well [5,15,16], no theoretical treatment incorporating the effects of the surface energy anisotropy on aggregate shape exists. We thus use a mean-field approach to estimate $\delta\mathbf{m}$ for a homogeneous ellipsoid with uniform polarization as $\delta\mathbf{m}=\mu_0 V_d\chi_d\delta\mathbf{H}$, where V_d is the droplet volume and $\delta\mathbf{H}$ is the difference between the local field in a bulk droplet and a surface droplet. Since the internal field in a spherical droplet arising from the uniform magnetization $\mathbf{M}$ of the surrounding media is $\mathbf{M}/3$, $\delta\mathbf{H}$ can be approximated as $\mathbf{M}/6\chi_a$, where $\mathbf{M}=\mathbf{m}_h/\mu_0 V_a$. Making the substitution $\phi_a=V_d N_d/V_a$ thus gives

$$\mathbf{m}_s=n_\sigma\mathbf{m}_h \quad \text{with } n_\sigma=\frac{N_s}{N_d}\frac{\chi_d\phi_a}{6\chi_a}, \tag{8}$$

where N_d is the number of droplets in the aggregate. The total aggregate dipole moment then becomes

$$\mathbf{m}_a=\mathbf{m}_h(1-n_\sigma). \tag{9}$$

In calculating n_σ, we estimate the ratio N_s/N_d by assuming uniform droplet density within the aggregate so that $N_s/N_d=V_s/V_a$, where $V_a=\frac{4}{3}\pi abc$ is the volume of the aggregate and $V_s=\frac{4}{3}\pi abc-\frac{4}{3}\pi(a-2r)(b-2r)(c-2r)$ is the volume occupied by the surface layer of particles.

The repulsive interactions between the aggregates also alters $\mathbf{m}_a$. When these interaggregate repulsive forces are taken into account, the homogeneous magnetic moment $\mathbf{m}_h$ of an aggregate surrounded by ellipsoidal aggregates, each with total dipole moment $\mathbf{m}_a$, becomes [8]

$$\mathbf{m}_h=\alpha\left(\mu_0 H-\sum_j T_{ij}\mathbf{m}_a\right). \tag{10}$$

The polarizability α is equal to $\mathbf{m}_h/\mu_0\mathbf{H}$ for an isolated aggregate and can be determined from Eq. (4). The quantity T_{ij} describes the field experienced by aggregate i due to an aggregate j a distance d_{ij} away. In the dipolar approximation, where each aggregate's polarization is concentrated entirely on its revolution axis, T_{ij} is given by

$$T_{ij}=\frac{1}{4a^2}\left[\frac{2}{d_{ij}}-\frac{2}{(d_{ij}^2+4a^2)^{1/2}}\right]. \tag{11}$$

Since our objective is to incorporate the effects of neighboring aggregates on the most energetically favorable ellipsoid eccentricity for the experimental conditions of Fig. 1, rather than examine the effects of interaggregate repulsion on aggregate spacing, we fix the interaggregate separation d_0 to be 32 μm, the experimentally observed average aggregate separation distance. To calculate $\Sigma_j T_{ij}$, we sum the contribution from pairs of aggregates with $d_{ij}=nd_0$ for the nth pair until the contribution becomes negligible.

An equation for the total suspension energy incorporating the effects of the demagnetizing field, the surface energy and the repulsive interaction between aggregates can now be written. Solving Eqs. (9) and (10) simultaneously yields the total aggregate dipole moment $\mathbf{m}_a$. Using the resulting expression for $\mathbf{m}_a$ in Eq. (3) and making the substitution $NV_a/V=\phi/\phi_a$ then gives

$$\frac{U_T}{V}=-\frac{\phi H^2}{2\phi_a}\left[\frac{\mu_0\chi_a}{1+(4\pi\chi_a)n_z}\right]\left[\frac{1-n_\sigma}{1+n_r(1-n_\sigma)}\right], \tag{12}$$

with $n_r=\alpha\Sigma_j T_{ij}$.

Preliminary calculations using Eq. (12) show that the most energetically favorable ellipsoid width-to-length ratio b/a exhibits a sensitive dependence on the ellipsoid semithickness c. As mentioned previously, we could not determine the value of c experimentally. Since the ferrofluid-containing droplets are much heavier than water, having a density of 1.56 g/cm^3, and the aggregates are resting on the bottom of the sample holder, we felt it necessary to include the effects of gravity on aggregate shape in case gravity was influencing aggregate thickness.

To incorporate gravitational effects, we treat the aggregate as a series of layers, each one-particle diameter in height. We estimate N_l, the number of particles in layer l by calculating the volume of layer l, dividing by the total aggregate volume and multiplying by N_d the total number of droplets in the aggregate. The energy of the aggregate due to gravitational effects U_G is then

$$U_G=\sum_l (\rho_d-\rho_w)V_d g h_l N_l, \tag{13}$$

where $\rho_d-\rho_w$ is the density difference between a droplet and water, $V_d=\frac{4}{3}\pi r^3$ is the droplet volume, g is the gravitational acceleration, and $h_l=2r(l-1)$ is the distance from the bottom of layer l to the aggregate bottom. Multiplying Eq. (13) by N/V gives the total gravitational contribution to the suspension energy per volume. Adding the gravitational energy to the dipolar energy in Eq. (12) and substituting $\phi/V_a\phi_a$ for N/V yields the final expression for the total energy of the suspension per volume:

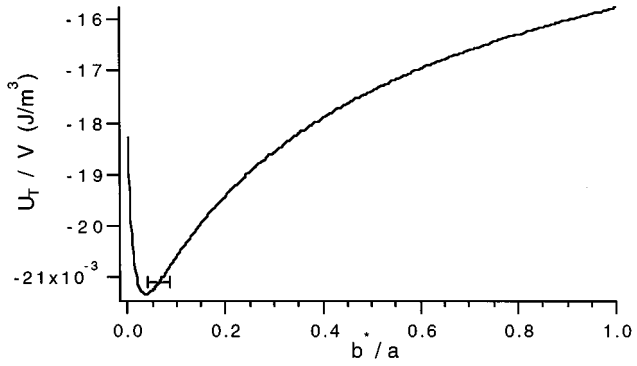

FIG. 5. Total energy per suspension volume as a function of b^*/a, the lowest energy b to a ratio for each given value of b (i.e., the total energy is a function of c as well as b/a), for particles with $r = 0.32\ \mu$m and $\chi = 2.2$ and an aggregate volume of 2800 μm^3. The bar indicates the average experimentally observed b/a values.

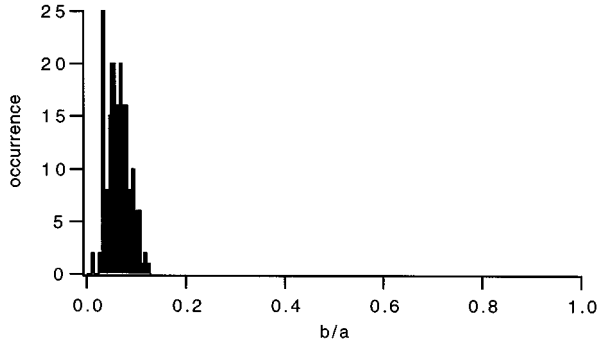

FIG. 6. Histogram of experimental b/a values for aggregates formed under the same experimental conditions as in Fig. 5.

$$\frac{U_T}{V} = -\frac{\phi H^2}{2\phi_a}\left[\frac{\mu_0\chi_a}{1+(4\pi\chi_a)n_z}\right]\left[\frac{1-n_\sigma}{1+n_r(1-n_\sigma)}\right]+\frac{\phi U_G}{V_a\phi_a}. \tag{14}$$

C. Calculations: Results and discussion

To predict the most energetically favorable aggregate shape, we used Eq. (14) to compute U_T/V for all possible aggregate shapes for an aggregate of constant volume V_a. Beginning with the thinnest possible ellipsoid ($b=r$), we slowly increased the aggregate semiwidth b until $b=a$. For each value of b, we calculated U_T/V for every possible combination of c and a that satisfied the constant volume requirement and the requirement that $a \geq b \geq c \geq r$.

In Fig. 5 we plot U_T/V versus b^*/a, where b^*/a is the lowest energy b to a ratio corresponding to a given b value. Note that solving for U_T/V as a function of b^*/a does not constrain c to be a constant or a predetermined function of b, but rather allows for a global minimization of energy by considering all possible ellipsoidal shapes. The variation in the most energetically favorable aggregate semithickness c^* with b^*/a will be discussed below.

The values plotted in Fig. 5 are for a particle radius of 0.32 μm, a droplet magnetic susceptibility of 2.2, and an aggregate volume of 2800 μm^3, the average estimated volume of the aggregates that form under the experimental conditions of Fig. 1. We chose to analyze aggregates of this relatively low volume because larger aggregates develop multiple spikes per end and thus deviate further from our ellipsoidal model. The smallest b^*/a value in Fig. 5 corresponds to a fully elongated ellipsoid, one that spans the 1 cm cell width. The energetic minimum occurs at a b^*/a value of 0.037 with $a=81.0\ \mu$m, $b=3.02\ \mu$m, and $c=2.71\ \mu$m.

A histogram of experimental b/a values for aggregates formed under these experimental conditions is shown on the same scale in Fig. 6. The average experimental value $b/a=0.063\pm0.0235$ is shown in Fig. 5 for comparison with the theoretically predicted energetic minimum. Figures 5 and 6 thus show that the lowest-energy aggregate shape predicted by the theory is slightly more elongated than the average experimental value, but still well within the range of shapes observed experimentally. This close agreement between theory and experiment is very promising and supports the validity of this model based on the competition between surface energy, the demagnetizing field, and interaggregate repulsion.

We note that a more exact agreement between the theoretically predicted lowest-energy b/a value and the average experimental b/a value cannot reasonably be expected, given the limitations of the theory. In order to calculate the demagnetizing field, it was necessary to model the aggregates as ellipsoids. Figure 2 clearly shows, however, that the aggregates are not perfect ellipsoids, having conical ends in the field direction rather than a uniformly smooth surface. These conical tips cannot be incorporated into the theory, but do alter the interplay of the demagnetizing field and surface energy in the end region. Furthermore, only an isotropic expression for the surface energy could be included in the theory since no analytical treatment incorporating the influence of the anisotropic nature of the surface energy on aggregate shape exists. Thus the b/a value corresponding to the theoretical energy minimum should be regarded more as a reasonable approximation than as a precise prediction of the equilibrium aggregate shape.

It is useful to examine the contributions from gravity and the three dipolar energies to the curve in Fig. 5 to assess the relative significance of each component. Analysis of the gravitational term $\phi U_G/V_a\phi_a$ indicates that the total energy exceeds the gravitational energy by approximately two orders of magnitude and the effect of gravity on aggregate shape is very minor and can essentially be regarded as a slight perturbation to the total-energy curve.

The first expression on the right-hand side of Eq. (14) contains the energetic contributions from each of the three dipolar interactions. From analysis of this expression, we see that the term $-\phi H^2\mu_0\chi_a/2\phi_a$ is independent of aggregate shape and represents the suspension energy at its minimum (i.e., when no dipolar interactions are present and n_z, n_σ, and $n_r=0$). The term $1/[1+(4\pi\chi_a)n_z]$ contains the effects of the demagnetizing field on aggregate shape, the term $1-n_\sigma$ represents the surface energy effects on aggregate shape, and $1/[1+n_r(1-n_\sigma)]$ is a term incorporating the contribution from the interaggregate repulsive interaction. Plots of the product of each of these three multiplicative factors and the shape independent factor $-\phi H^2\mu_0\chi_a/2\phi_a$ are shown in Fig. 7. Each plot is equivalent to the suspension energy when only the specified dipolar interaction is in-

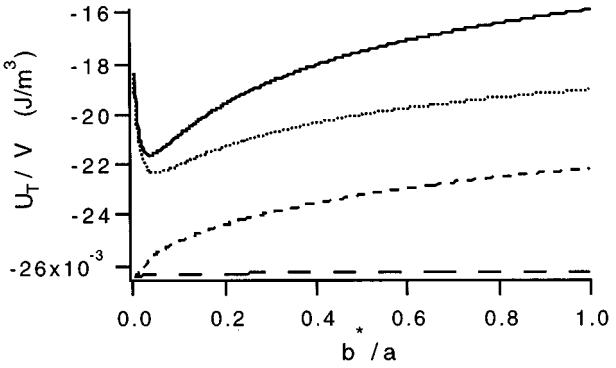

FIG. 7. Calculated suspension energy when the effects of the interaggregate repulsion (— —), the surface energy (· · ·) and the demagnetizing field (- - -) are considered separately and when all three dipolar effects are included together (——), plotted as a function of b^*/a, the lowest energy b to a ratio for each given value of b. Gravitational effects are not included in these calculations.

cluded and thus illustrates the relative influence of each dipolar interaction on the shape of the total-energy curve. The total suspension energy when all three dipolar forces are included is also shown in Fig. 7. Gravitational effects are not included in these calculations in order to isolate the effect of each dipolar force on aggregate shape. For comparison, if no dipolar interactions are considered, the total suspension energy has a value of $-0.0264\ J/m^3$ and is invariant with aggregate aspect ratio. Each dipolar interaction thus increases the suspension energy, although the increase is minimal in the case of the interaggregate repulsion.

The amount of influence a specific dipolar interaction has on aggregate shape is indicated by the degree of variation of the corresponding energy curve with b^*/a. Figure 7 thus illustrates that for the experimental conditions specified in these calculations, the repulsive interaction between aggregates is relatively insignificant and aggregate shape is determined primarily by the competition between surface energy and demagnetizing field effects. The surface effects dominate the shape of the total-energy curve at elongated shapes, while the demagnetizing field effects become more significant at larger b^*/a values. The total energy plotted in Fig. 5 thus initially decreases with increasing b^*/a at low b^*/a values

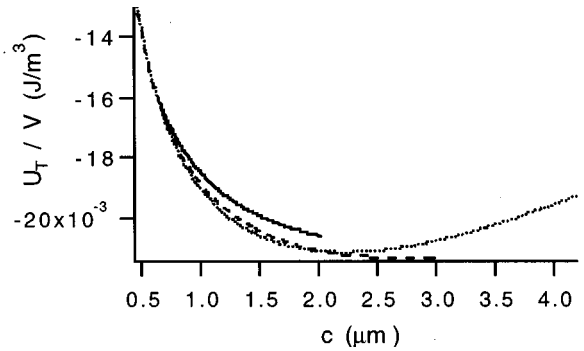

FIG. 8. Total suspension energy per volume as a function of the aggregate semithickness c for aggregate semiwidth values of $b=2.02\ \mu$m (——), $b=3.02\mu$m (- - -), and $b=4.22\mu$m (· · ·).

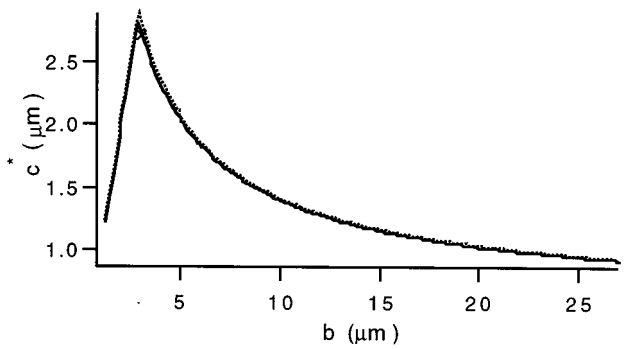

FIG. 9. The most energetically favorable value of the aggregate semiwidth c^* as a function of the aggregate semiwidth b with (——) and without (· · ·) the effects of gravity. The × marks the point corresponding to the lowest-energy values of b and c ($b^*=3.02\ \mu$m and $c^*=2.71\ \mu$m).

where the surface energy dominates and favors a more spherical shape, but eventually increases with b^*/a when the demagnetizing field becomes the more dominant effect and favors a more elongated aggregate shape. The b/a value corresponding to the energetic minimum is thus determined by the crossover between the dominance of surface energy and demagnetizing field effects.

A similar explanation accounts for the aggregate thickness. Figure 8 shows the total energy per suspension volume as a function of aggregate semithickness c for three values of the ellipsoid semiwidth b. Surface effects dominate at small c values, causing the energy to decrease with increasing c, until demagnetizing effects take over and, aided slightly by gravitational effects, cause an increase in energy with c. The crossover point between the dominance of demagnetizing field and surface effects, which determines the most energetically favorable aggregate thickness, shifts to lower c values as b increases. This shift accounts for the decrease in the most favorable semithickness c^* as b increases in the latter part of the c^* versus b curve plotted in Fig. 9. The initial increase in c^* with b in Fig. 9 arises from the fact that at small b values, the crossover point is never reached, as illustrated by the $b=2.02\ \mu$m curve in Fig. 8, and thus the most favorable semithickness c^* occurs when $c=b$. The dashed line in Fig. 9 shows the shape of the c^* versus b curve when gravitational effects are neglected and demonstrates the relatively minor effects of gravity on aggregate thickness. The point corresponding to the lowest-energy b and c values, ($b^*=3.02\ \mu$m and $c^*=2.71\ \mu$m) is marked on Fig. 9 and occurs just after the peak in the c^* versus b curve. It is interesting to note that at this aggregate volume, c^* would equal b^*, and the most favorable aggregate shape would be an ellipsoid of revolution, were it not for the slight perturbative effects of gravity.

The decrease in c^* with increasing b and thus b^*/a explains the decrease in the surface energy factor in Fig. 7 at large b^*/a values. If c were constant, the surface energy factor $1-n_\sigma$ would increase continuously with b/a since the surface energy favors adoption of a more spherical shape, but the decrease in c^* with b^*/a is accompanied by a surface energy penalty that overrides the benefit gained from the increase in the aggregate width to length ratio.

At larger aggregate volumes, the aggregate ends develop multiple spikes and can no longer be accurately modeled as ellipsoids. No comparison can therefore be made between the theoretical predictions and experimental measurements of aggregate shape for these larger aggregate volumes. Equation (14) does indicate, however, that the total suspension energy U_T/V will decrease when larger aggregates are formed. This trend is supported by the Clausius-Mosotti relation [7] and our observations that aggregates always continue to grow over the course of an experiment, but never break apart to form two smaller aggregates.

Studies with droplets smaller than 0.26 μm in radius show a substantially different structural evolution than that illustrated in Fig. 1. Instead of relaxing into ellipsoidal aggregates that are detached from the cell walls, the smaller droplets form very thin, evenly spaced columns that remain fully extended across the length of the cell. Equation (14) provides a qualitative explanation of this trend, predicting more elongated aggregates for smaller droplets. This dependence of shape on droplet size arises from the fact that the demagnetizing field is invariant with droplet size, while N_s/N_p and hence n_σ are proportional to the droplet radius r. As droplet size decreases, the surface energy effects thus diminish, allowing the relatively greater demagnetizing field effects to have a more dominant influence on aggregate shape and resulting in more elongated aggregates. The very sudden transition in suspension structure from detached ellipsoids to fully extended columns as droplet size decreases from 0.32 μm to 0.26 μm is not captured by Eq. (14), however, which predicts a much more gradual aggregate elongation. At $r=0.01$ μm, Eq. (14) yields a most favorable b/a value of 7.3×10^{-3}, corresponding to an aggregate length $2a$ of 580 μm, which is just shy of full elongation across the cell.

III. AGGREGATE END STRUCTURE

The low-energy MR fluid aggregates that form in a pulsed magnetic field have an intriguing end structure. In Fig. 2 it can be seen that instead of adopting a smooth ellipsoidal shape, the aggregates develop conical tips in the field direction. This preference for spiked ends is even more dramatic in the larger aggregates formed at higher concentrations, as illustrated in Fig. 10(a), which shows the end structure of a sample with a droplet volume fraction of 0.02 after exposure to a strong magnetic field ($\lambda=37$), pulsed at a frequency of $\nu = 2$ Hz, for 1 h.

It should be noted that the formation of the conical spikes is frequency dependent; at low frequencies the end structure comprises chainlike projections rather than conical spikes, as shown in Fig. 10(b). At low frequencies the end structure completely dissolves during each field-off pulse due to Brownian motion of the surface droplets. When the field is reapplied, the droplets undergo a kinetically driven organization into the chainlike projections shown in Fig. 10(b). In contrast, at higher frequencies, the droplet diffusion distance during the field-off pulses is not great enough to erase the end structure and a minimization of energy through rearrangement into conical spikes can occur. The transition between frequencies that produce chainlike projections and conical spikes is determined by the average droplet diffusion

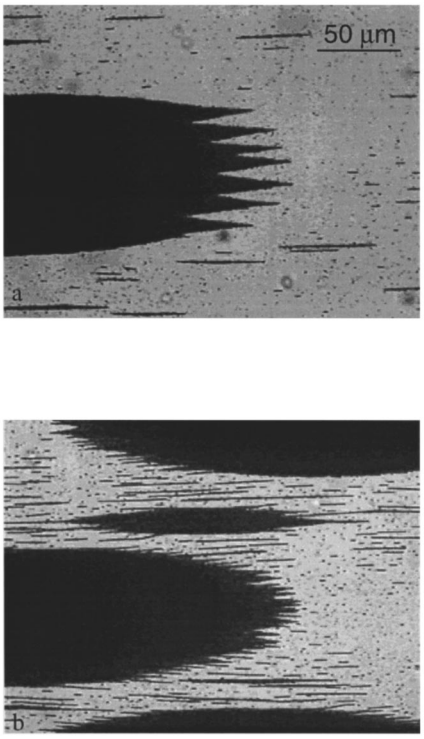

FIG. 10. Ends of the ellipsoidal aggregates formed in a suspension ($\phi = 0.02$ and $r=0.32$ μm) exposed to a strong ($\lambda=37$) pulsed magnetic field of pulse frequency (a) 2 and (b) 0.2 Hz. Each suspension has been in the pulsed field for 1 h and the structures have achieved their final form.

distance in the field-off state $\langle x^2\rangle^{1/2}$ and occurs at $\langle x^2\rangle^{1/2}\sim0.8$ μm [4].

Although inaccessible at low frequencies, conical spikes appear to be the lowest-energy aggregate end structure. In addition, Fig. 10(a) demonstrates that not only are conical spikes favored over a smooth interface, but the range of spike sizes and angles is limited. Instead of forming just one conical tip per end that widens as the aggregate grows, the aggregate end consists of many small conical spikes of very similar size and cone angle. To quantify this preference for conical spikes of a certain size, in Fig. 11 we present a histogram of conical half angles α for two pulse frequencies $\nu = 2$ and 10 Hz. The conical half angle α is the angle

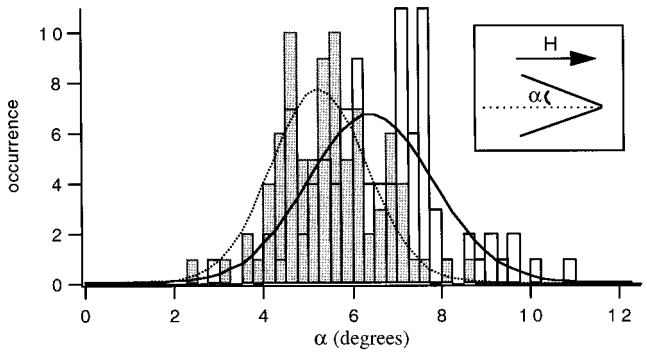

FIG. 11. Histogram of experimentally measured conical half angles for pulse frequencies of 2 Hz (unfilled bars) and 10 Hz (filled bars). Gaussian fits to the 2-Hz and 10-Hz data sets are given by —– and · · ·, respectively.

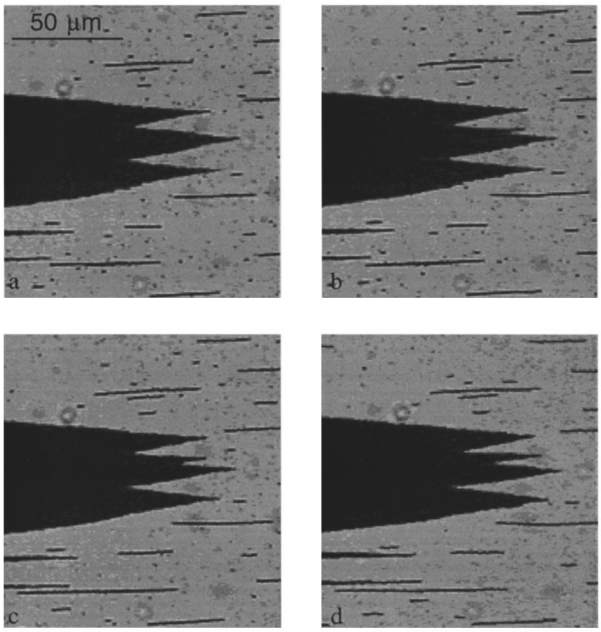

FIG. 12. Process of spike division. The pulse frequency of the field is 10 Hz and the middle spike of the aggregate in (a) is unstable, having an α value of 8.5°. (b)–(d) show the same aggregate (b) 15 s, (c) 75 s, and (d) 245 s later as the middle spike divides in two.

between the field direction and one of the faces of the conical spikes, as illustrated by the inset in Fig. 11.

Figure 11 shows that only conical spikes with $\alpha \leqslant 11°$ are formed in our experiments. From observation of the aggregate growth process, it can be seen that whenever large spikes approach the upper limit of allowable angles, they become unstable and divide into two smaller spikes, suggesting that an energetic penalty exists for large spikes. This spike division occurs over several minutes and takes place by a budding process off the side of the spike, where the angle between the conical surface and the field direction is greatest, rather than through tip splitting. Spike division begins with the formation of a thin chain that is attached to the side of the conical spike but aligned with the field direction rather than the spike surface. The existence of the small chain is tenuous; it is often reabsorbed by the original spike during subsequent pulses, only to form again almost immediately. Eventually, however, the small chain begins to grow at the expense of the original spike and the end result is two spikes that are well within the boundaries of allowable spike angles. This process is illustrated in Fig. 12.

This strong preference for conical spikes of a certain size, and thus for aggregate surfaces with a specific orientation relative to the field direction, derives from the surface energy anisotropy that favors some surface directions over others. Several theoretical studies of the surface energy of dipolar lattices have calculated a negative surface energy for surfaces perpendicular to the field direction [5,15,16]. These studies suggest that such surfaces would be unstable and hence forbidden since a stable interface between two phases requires a positive free energy of formation in order to prevent a continuous expansion of the surface region and an eventual complete mixing of the two phases [17]. Our experiments support this interpretation; in all of the experimental images shown in this paper, the field direction is along the long axis of the aggregates and it can be seen that no surfaces perpendicular to the applied field exist. In fact, it is by the formation of the conical spikes that the aggregate is able to circumvent having surfaces perpendicular to the field, while still adopting an ellipsoidlike shape.

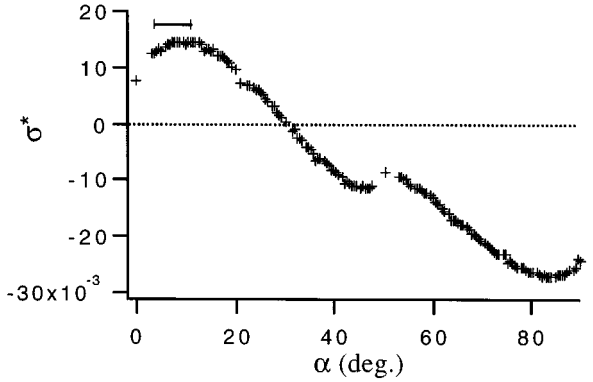

FIG. 13. Dimensionless surface energy σ^* as a function of the angle α the surface makes with the field direction for a body-centered tetragonal lattice structure. The surface energy calculations were done by Lobkovsky and Halsey [5]. The bar indicates the range of α values observed experimentally.

Lobkovsky and Halsey recently calculated the surface energy as a function of the surface orientation with respect to the dipole direction for several dipolar lattice structures, including body-centered-tetragonal (bct), face-centered-cubic (fcc), body-centered-cubic (bcc), and simple cubic structures [5]. Theoretical models have found that the bct structure has the lowest energy [16,18] and this prediction has been upheld in experiments by Chen *et al.* that identified the lattice structure adopted by a suspension of dipolar spheres as bct [19]. We should note, however, that the predicted energy differences between the bct and other close-packed lattice structures, namely, fcc and hcp, are small, approximately 6%, so that other effects, such as entropic considerations, could influence aggregate structure. While a bcc structure is reasonably close in energy to the close-packed structures, the simple cubic has a significantly higher energy and thus we will not discuss it in this analysis.

For a bct lattice, Lobkovsky and Halsey calculated that only surfaces with $\alpha \leqslant 31°$ have a positive surface energy, as illustrated in Fig. 13. Our experimental observations support this result since we observe no surfaces that form an angle with the applied field direction of more than 31°. The calculated surface energy curve for the bct has a broad peak at approximately $7° \leqslant \alpha \leqslant 13°$ and drops off on both sides of the peak fairly rapidly. The peak overlaps significantly with the experimentally observed values of α. At $\nu = 2$ Hz, the average experimental value is $\alpha = 6.5° \pm 1.5°$ and the experimental range of α values observed is $3° \leqslant \alpha \leqslant 11°$; for comparison with the calculated surface energies, this experimental range is shown by the horizontal bar in Fig. 13.

This correlation between the surface directions corresponding to the peak of the calculated surface energy curve and the experimentally observed values of α could be due to the instability of surfaces with lower energies. The maximum surface energy calculated for the bct lattice over the area of a

0.32-μm particle in a 1500-A/m field is approximately 90 kT. At the same field strength, the maximum dipolar interaction between two 0.32-μm particles (i.e., the force driving the formation of chains aligned with the field) is 38 kT. If the ratio of the surface energy to the dipolar chaining energy must be greater than 2 to form a stable surface, then according to the calculated surface energies, only those surfaces near the peak of the surface energy curve could exist. Specifically, only spikes with conical half angles in the range $3 \leqslant \alpha \leqslant 17$ would be stable. This analysis is supported by the division of conical spikes as they grow beyond a certain cone angle. As the cone angle increases beyond the range corresponding to the maximum surface energy, the energy of the spike surface decreases, falling below that required to maintain a stable surface. The surface energy is then comparable to the dipolar energy driving the chaining process and the first stage of spike division, the formation of a thin chain aligned with the field on the side of the spike surface, begins.

This ratio of the surface to chaining energies is independent of field strength and particle size. The surface energy for the area of a particle is $\sigma^*(\mu^2/\mu_0 r^5)\pi r^2$, where σ^* is the dimensionless surface energy calculated by Lobkovsky and Halsey. The magnetic chaining energy is given by $U_{\max}$ and can be obtained from Eq. (1) with $\theta = 0$ and $x = 2r$. The ratio of the two energies reduces simply to $(4\pi)^2\sigma^*$. This invariance of the ratio with respect to field strength and particle size is supported by our experimental observations since we find no dependence of the range of allowable spike sizes on field strength or particle size.

The agreement between the observed cone angles and the surface energy calculations is comparable for the fcc and bcc structures. The peaks in the surface energy curves for the fcc and bcc lattice structures are narrower and occur at α values of approximately 5 and 6, respectively [5]. The peak surface energies calculated for the fcc and bcc are slightly greater than for the bct. If a surface energy to chaining energy ratio greater than 2 is the criterion for surface stability, then surfaces with $\alpha \leqslant 20°$ could exist in a fcc lattice structure and surfaces with $\alpha \leqslant 16°$ would be stable in a bcc structure. These differences between the various lattice structures indicate the sensitivity of the surface energy to the precise structure of the aggregate.

Figure 11 also demonstrates that there is a slight dependence of spike angle on pulse frequency. When the field is pulsed at 10 Hz, instead of 2 Hz, the distribution of conical half angles observed is narrower. Specifically, the maximum observed spike angle decreases from 11° to 8.5°. To verify this frequency dependence, we monitored the cone angle on a single aggregate while switching the pulse frequency between 2 and 10 Hz. When we started with an aggregate exposed to a field pulsed at 2 Hz, then increased the frequency to 10 Hz, and allowed the end structure to equilibrate, we found that very large spikes ($\alpha \geqslant 7.5°$) in the initial end structure would split, while the rest of the spikes remained unchanged, as illustrated in Fig. 14. In going from $\nu = 2$ Hz in Fig. 14(a) to $\nu = 10$ Hz in Fig. 14(b), the largest spike divides while the rest of the end structure remains unaltered. Prior to division, the large spike had a half-angle value of $\alpha = 8°$, which is at the upper limit of the distribution observed for $\nu = 10$ Hz in Fig. 11. When the pulse frequency is returned to $\nu = 2$ Hz in Fig. 14(c), the original spike pattern is reformed. One explanation for this dependence of spike angle on pulse frequency could be that the pulse frequency influences the structure of droplets within the spikes, thereby impacting the most favorable surface direction since the surface energy is very sensitive to the precise structure of the aggregate.

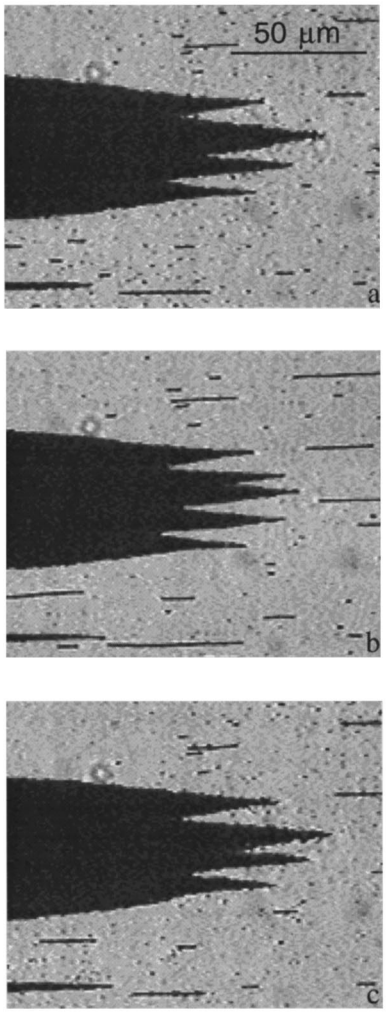

FIG. 14. (a) The aggregate is in a field with pulse frequency 2 Hz and all of the conical spikes are stable. (b) Upon increasing the pulse frequency to 10 Hz, the largest spike in (a) ($\alpha = 8°$) becomes unstable and undergoes spike division. (c) When the frequency is returned to 2 Hz, the original end structure is regenerated.

IV. CONCLUSION

We have shown that the application of a pulsed magnetic field to a magnetorheological fluid produces a low-energy suspension structure by allowing minimization of energy through structural rearrangements during the field-off pulses. We have analyzed the low-energy suspension structure comprising ellipsoidal aggregates with conical tips to determine the primary forces influencing aggregate shape. Modeling the smaller aggregates that form in low-concentration suspensions as ellipsoids, we calculated the equilibrium aggregate aspect ratio based on the competing effects of the demagnetizing field, surface energy, interaggregate repulsion, and gravity. The most favorable aggregate shape predicted

by these calculations was just slightly more elongated than the average experimental value, but well within the range of shapes observed experimentally. This close agreement between theory and experiment confirmed that aggregate shape is determined primarily by a competition between the demagnetizing field and surface effects since the interaggregate repulsion and gravitational effects proved to be very minor for these experimental conditions.

An analysis of surface energy anisotropy calculations for dipolar lattice structures suggests that the formation of conical spikes derives from the negative surface energy, and thus instability, of surfaces perpendicular to the field direction. A comparison of our experimentally observed range of conical half angles with calculations of surface energy as a function of angle with the field direction indicates that surfaces can exist only if the ratio of the surface energy to the dipolar chaining energy is great enough to ensure stability. When spikes grow beyond angles corresponding to the peak in the surface energy curve, the energy of the spike surfaces decreases and becomes comparable to the energy driving the formation of chains aligned with the field. The spike then becomes unstable and divides into two smaller spikes having greater surface energies. We observe a slight dependence of the maximum allowable spike size on pulse frequency. This dependence could indicate that the pulse frequency is influencing the internal structure of the spikes, and thereby the spike stability, since the surface energy is quite sensitive to the structure of droplets within a spike.

ACKNOWLEDGMENTS

We are grateful to T. Halsey for stimulating discussions regarding the surface energy calculations and R. Reamey for his insights on the aggregate thickness. We would like to thank J. Bibette for the donation of the ferrofluid and Bénédicte Deminière for her valuable assistance with the emulsion synthesis and fractionation. This work was supported in part by the Stanford Integrated Manufacturing Association, the Department of Defense, and an AT&T GRPW grant.

[1] J. Rabinow, AIEE Trans. **67**, 1308 (1948).
[2] W. Leventon, Design News **1993**, 185.
[3] J. D. Carlson and K. D. Weiss, Machine Design **1994**, 61.
[4] J. H. E. Promislow and A. P. Gast, Langmuir **12**, 4095 (1996).
[5] A. E. Lobkovsky and T. C. Halsey, J. Chem. Phys. **103**, 3737 (1995).
[6] J. Bibette, J. Colloid Interface Sci. **147**, 474 (1991).
[7] T. C. Halsey and W. Toor, Phys. Rev. Lett. **65**, 2820 (1990).
[8] Y. Grasselli, G. Bossis, and E. Lemaire, J. Phys. (France) II **4**, 253 (1994).
[9] E. Lemaire, Y. Grasselli, and G. Bossis, J. Phys. (France) II **2**, 359 (1992).
[10] J. Liu, E. M. Lawrence, A. Wu, M. L. Ivey, G. A. Flores, K. Javier, J. Bibette, and J. Richard, Phys. Rev. Lett. **74**, 2828 (1995).
[11] L. D. Landau, E. M. Lifshitz, and L. P. Pitaevskii, *Electrodynamics of Continuous Media*, 2nd ed. (Pergamon, New York, 1984).
[12] G. Bánhegyi, Colloid Polymer Sci. **266**, 11 (1988).
[13] E. C. Stoner, Philos. Mag. **36**, 803 (1945).
[14] *Handbook of Mathematical Functions*, edited by M. Abramowitz and I. A. Stegun (Dover, New York, 1970).
[15] H. J. H. Clercx and G. Bossis, J. Chem. Phys. **98**, 8284 (1993).
[16] W. R. Toor and T. C. Halsey, Phys. Rev. A **45**, 8617 (1992).
[17] A. W. Adamson, *Physical Chemistry of Surfaces*, 5th ed. (Wiley, New York, 1990).
[18] R. Tao and J. M. Sun, Phys. Rev. Lett. **67**, 398 (1991).
[19] T. Chen, R. N. Zitter, and R. Tao, Phys. Rev. Lett. **68**, 2555 (1992).